Research on Engineering Structures & Materials
www.jresm.org
MIM Research Group

Research Article

Research on a multi-factor time-varying prediction model for the corrosion rate of reinforcing bars in existing concrete structures

Liying Zhu [*,a], Weizhong Wang [b], Haiyong Cai [c], Fang Jin [d]

College of Engineering, Huanghe Science and Technology College, ZhengZhou, 450063, China

Article Info

Article History:

Received 07 Jul 2026

Accepted 22 Sep 2026

Keywords:

Reinforcing bar corrosion; Multi-factor coupling; Time-varying prediction model; Concrete deterioration; Durability assessment

Abstract

The corrosion of reinforcing bars in existing concrete structures exhibits strong time-varying characteristics under the combined action of multiple factors. Most existing corrosion rate prediction models rely on single-factor or static analyses. They are insufficient for accurately depicting the coupling of multiple factors and the law of time-series evolution, and they also exhibit deficiencies in prediction accuracy and adaptability to actual projects. Starting from the electrochemical nature of rebar corrosion, this paper systematically analyses the mechanisms that induce concrete deterioration during corrosion initiation and development, identifies key influencing variables, including environmental factors, material properties, structural characteristics, and crack evolution, and constructs a computer model of the coupling relationships among multiple factors. In combination with the time-series evolution law of the corrosion rate, a multi-factor features input module and a time-series feature fusion mechanism are established to achieve the in-depth integration of static and dynamic features, thereby forming a time-varying prediction model that considers both mechanism constraints and has data-driven capabilities. The results of multi-factor coupling prediction show that the rate deviation is 8.9 μA/cm^2 under the weak-coupling condition, the model feature matching degree is 67.5%; the average rate is 72.3 μA/cm^2 under the medium-coupling condition, the fitting degree of time-varying features is 49.1%; the fitting accuracy under strong coupling is 88.7%, the proportion of load - coupling influence is 23.6%, the comprehensive prediction relative error is 59.8‰, and the global prediction accuracy of the model reaches 97.4%, indicating a stable time-varying prediction effect.

© 2026 MIM Research Group. All rights reserved.

1. Introduction

In the early development stage of concrete structures, people's understanding of concrete materials mainly remained at the compositional level. It was generally believed that concrete was composed of natural aggregates such as cement, pebbles, and sand [1, 2]. Specifically, Xi et al. [1] established an accurate cover crack modeling method for reinforced concrete structures under non-uniform corrosion, and revealed the quantitative relationship between corrosion expansion force and crack propagation path. Yang et al. [2] proposed an analytical model for concrete cracking induced by non-uniform corrosion, and derived the critical corrosion amount corresponding to initial cracking of the cover layer. These materials showed high stability and durability in the natural environment. For a long time, the engineering community has held the view that concrete structures are inherently durable and not prone to significant deterioration [3, 4]. Maric et al. [3] evaluated reinforcement corrosion and concrete damage on bridges using non-destructive testing

*Corresponding author: liyingzhu2026@outlook.com
[a]orcid.org/ 0009-0000-4995-3177; [b]orcid.org/ 0009-0005-5149-3399; [c]orcid.org/0009-0003-2499-6666; [d]orcid.org/0009-0004-4370-737X
DOI: http://dx.doi.org/10.17515/resm2026-1834st0707rs

technology, and confirmed that corrosion-induced damage is the main cause of durability degradation of in-service bridges. In this cognitive framework, although steel bars were introduced as the core load-bearing material, they were tightly wrapped in concrete and not directly exposed to air or moisture. People often ignored their potential corrosion risks [5]. In addition, the high alkalinity of the concrete could form a passive film on the steel bars' surfaces, strengthening confidence in their durability [6, 7]. In engineering practice, it was generally believed that reinforced concrete structures did not require special durability design and post-maintenance, as long as they met the requirements of strength and bearing capacity [8]. With the widespread application of reinforced concrete structures in various engineering projects and the advancement of long-term service practice, durability problems in these structures have gradually emerged under complex environmental conditions [9, 10]. In marine environments, saline-soil areas, and urban areas affected by industrial pollution, the protective performance of concrete has been continuously weakened by chloride-ion intrusion and carbon dioxide carbonation, gradually destroying the passive film on the surface of steel bars and leading to corrosion reactions [11]. The volume expansion caused by corrosion of steel bars leads to cracking and spalling of the protective layer, further reducing the section, weakening the bonding performance, and degrading the bearing capacity. A large number of existing engineering examples demonstrate that steel bar corrosion is a key factor affecting the durability and safety of concrete structures [12, 13].

Compared with previous studies, the novel aspects of this work are mainly reflected in the following three aspects. First, unlike traditional studies that analyze environmental erosion, stress loading, or crack development in isolation, our model establishes a multi-scale, multi-factor coupling mechanism that accounts for the mutual promotion between concrete matrix deterioration, interfacial shear degradation, and rust expansion, realizing the quantitative characterization of synergistic effects among multiple variables. Second, a time-series feature fusion mechanism is proposed, which divides the corrosion process into four stages according to the evolution law of electrochemical state, and realizes adaptive prediction of corrosion rate in different stages by combining static material parameters and dynamic environmental monitoring data.

In existing research, various technical approaches have been developed to predict the corrosion rate of steel bars, which can be mainly divided into three categories: mechanistic models, empirical models and data-driven intelligent models. Mechanistic models, represented by the classical Tuutti model and the Life-365 service life prediction framework, are usually based on electrochemical principles of steel bar corrosion, establishing a theoretical framework that accounts for chloride-ion diffusion, oxygen transfer, charge conservation, and polarization behavior. Such models emphasize the interpretability of physical and chemical processes, but most of them adopt simplified assumptions of uniform diffusion and static environment, making it difficult to characterize the time-varying coupling of multiple factors. Empirical models such as the DuraCrete model are established based on a large number of field exposure test data, which have strong engineering practicability, but their parameter universality is poor, and the prediction accuracy will decrease significantly when applied to regions or environments outside the database [14]. Mechanism models are usually based on electrochemical principles of steel bar corrosion, establishing a theoretical framework that accounts for chloride-ion diffusion, oxygen transfer, charge conservation, and polarization behavior. Such models emphasize the interpretability of physical and chemical processes and can reveal the essential mechanism of corrosion reactions [15, 16]. The corrosion of steel bars is often affected by multiple factors, including fluctuations in environmental temperature and humidity, evolution of concrete pore structure, crack development, external load effects, and differences in material properties [17, 18]. To simplify calculations and theoretical derivations, most mechanism models consider only one or a few influencing factors during the establishment process, thereby ignoring complex coupling effects among multiple factors [19]. The chloride-ion diffusion process is not only affected by concrete porosity but is also closely related to humidity cycles, temperature gradients, and microcrack development. There are obvious synergistic or inhibitory effects among these factors. Traditional mechanism models often deviate from the actual monitoring results in engineering applications.

2. Core Mechanism of Reinforcing Bar Corrosion in Existing Concrete Structures

2.1 Electrochemical Nature and Time-Series of Reinforcing Bar Corrosion

All equations from (1) to (13) are derived based on classical electrochemical principles, concrete mechanics theory and micromechanics framework, following a progressive logic from material performance degradation to structural response evolution. Equations (1) and (2) for concrete tensile strength are derived from the time-dependent degradation model of concrete mechanical properties, combined with the thick-walled cylinder stress formula under uniform radial expansion pressure. Equation (3) for bearing capacity is established based on the sectional analysis method of reinforced concrete members, introducing the corrosion current density term to characterize the attenuation of effective steel section and bond performance. Equation (4) for steel cross-section loss is derived directly from Faraday's law of electrolysis, which describes the quantitative relationship between charge transfer and metal mass loss. Equations (5) and (6) for passive film characteristics are established based on the dissolution kinetics of oxide film in alkaline environment and the adsorption mechanism of chloride ions on the film surface. Equations (7) and (8) for ion diffusion and passive current are derived from Fick's second law and the Butler-Volmer equation, considering the modification effect of pore structure and temperature on diffusion coefficient. Equations (9) to (12) for mesoscopic structure parameters are derived from the composite material mixing law and the interfacial transition zone strength model, which characterize the mechanical and transport properties of each phase inside concrete. Equation (13) for concrete deterioration degree is constructed based on the carbonation depth model and crack damage evolution theory, which quantifies the comprehensive degradation state of concrete protective layer.

Pressure causes tensile stress concentration in the protective layer around the steel bar. When the tensile stress exceeds the tensile strength of concrete [20, 21], the tensile strength equations are shown in Equations (1) and (2), where ft,t is the tensile strength of concrete at time t (MPa); ft0 is the initial tensile strength of concrete (MPa); t is the service time (years); hc is the thickness of the concrete protective layer (mm); p is the porosity of concrete (%); σt,max is the maximum tensile stress of concrete around the steel bar (MPa); Fc is the rust - expansion force (N); ds is the diameter of the steel bar (mm); Ac is the effective bearing area of concrete (mm^2); Ec is the elastic modulus of concrete (MPa); εcorr is the corrosion strain of the steel bar (%). Then micro - cracks will occur and gradually expand into through-cracks as the corrosion continues.

$$f_{t,t} = f_{t0} \times (1 - 0.012t) \times \sqrt{\frac{h_c}{25}} \times \left(1 - \frac{p}{40}\right) \tag{1}$$

$$\sigma_{t,max} = \frac{F_c \times d_s}{2 \times A_c \times h_c} + \frac{E_c \times \varepsilon_{corr} \times d_s}{2 \times h_c} \tag{2}$$

The formation of cracks not only weakens the overall stiffness and bearing capacity of the component, but also provides a more convenient passage for the intrusion of external moisture, oxygen, and chloride ions [22]. The bearing capacity equation is shown in Equation (3). Pu is the bearing capacity of the component at time t (kN); Pu0 is the initial bearing capacity (kN); wc is the current crack width (mm); w0 is the initial crack width (mm); Icorr is the steel corrosion current density ($\mu A/cm^2$). This forms a vicious circle and accelerates the corrosion rate.

$$P_u = P_u 0 \times \left[1 - 0.035 \times \sqrt{t} \times \left(\frac{w_c}{w_0} - 1\right) \times \frac{I_{corr}}{0.1}\right] \tag{3}$$

In terms of the degree of influence and scope of action, steel corrosion not only changes the local cross-section performance [23, 24]. The cross-section equation is shown in Equation (4). As,t is the effective cross-sectional area of the steel at time t (mm^2); As0 is the initial cross-sectional area of the steel (mm^2); τ is the integral time variable (years); Mfe is the molar mass of iron (g/mol); n is the number of electron transfers in the electrode reaction; F is the Faraday constant (C/mol); ρfe is the density of the steel (g/cm^3). It also affects the overall force-bearing system of the component. In severe cases, it may even lead to the premature failure of the structure and the early retirement

of the engineering project. It is necessary to deeply reveal the electrochemical nature of steel corrosion and its time-series evolution law.

$$A_s,t = A_s0 \times \exp\left(-\int_0^t \frac{I_{corr,\tau} \times M_{fe}}{n \times F \times \rho_{fe} \times 10^6} d\tau \right) \tag{4}$$

After the reinforced concrete structure is poured and undergoes initial curing, the cement hydration reaction gradually becomes sufficient, and an alkaline environment represented by calcium hydroxide is formed inside the concrete [25]. The film equations are shown in Equations (5) and (6). dm, t is the thickness of the passive film at time t (nm); dm0 is the initial thickness of the passive film (nm); pH is the pH value of the concrete pore solution. Rm, t is the resistance of the passive film at time t (Ω·cm^2); Rm0 is the initial resistance of the passive film (Ω·cm^2); Ccl is the chloride ion concentration in the concrete (%). The high - alkalinity conditions of the concrete pore solution cause a dense and stable oxide film to form rapidly on the surface of the steel. This film is usually called the passive film.

$$d_m,t = d_m0 \times \left(1 + 0.08 \times \ln\left(1 + t\right)\right) \times \left(\frac{pH}{13} \right)^{1.5} \tag{5}$$

$$R_m,t = R_m0 \times \frac{d_m,t}{d_m0} \times \left(1 - 0.02 \times C_{cl} \times t\right) \tag{6}$$

The existence of the passive film effectively blocks the direct contact between the steel and the external corrosion medium. The pore equations are shown in Equations (7) and (8). Dion,t is the diffusion coefficient of corrosion ions at time t (cm^2/s); Dion0 is the initial diffusion coefficient (cm^2/s); p0 is the initial porosity (%); wc is the moisture content of the concrete (%); T is the ambient temperature (°C). Ipass, t is the passive current density at time t (μA/cm^2); Ipass0 is the initial passive current density (μA/cm^2). This makes the steel in a relatively stable electrochemical state. Although the steel is immersed in the water - containing pore solution, due to the protective effect of the alkaline environment, its corrosion potential is maintained within a relatively stable range, and the corrosion current density is extremely low. It is considered to be in a passivated state.

$$D_{ion,t} = D_{ion0} \times \left(\frac{p}{p0} \right)^{2.3} \times \left(1 + 0.15 \times w_c\right) \times \exp\left(\frac{-2000}{273 + T} \right) \tag{7}$$

$$I_{pass,t} = I_{pass0} \times \left(\frac{R_m0}{R_m,t} \right) \times \left(1 - 0.01 \times \left(T - 20\right)\right) \times \sqrt{\frac{h_c}{30}} \tag{8}$$

2.2 Induction Mechanism and Quantitative Correlation of Concrete Deterioration to Steel Corrosion

From the mesoscopic level analysis, concrete is mainly composed of mortar matrix, coarse and fine aggregates, and the interfacial transition zone between aggregates and mortar. The interfacial transition zone is usually the weakest part of the structure. The equations of the transition zone are shown in Eqs. (9) and (10). pitz,t is the porosity (%) of the interfacial transition zone at time t; pitz0 is the initial porosity (%) of the interfacial transition zone; wb is the water-binder ratio. fitz,t is the tensile strength (MPa) of the interfacial transition zone at time t; fitz0 is the initial tensile strength (MPa) of the interfacial transition zone. It has a relatively high porosity, a relatively loose structure, and both mechanical and durability properties are lower than those of the matrix part.

$$p_{itz,t} = p_{itz0} \times \left(1 + 0.04 \times t^{0.6}\right) \times \left(\frac{w_b}{0.45} \right)^{1.2} \tag{9}$$

$$f_{itz,t} = f_{itz0} \times \left(1 - 0.05 \times \frac{p_{itz,t} - p_{itz0}}{p_{itz0}} \right) \times \left(1 - 0.02 \times C_{cl}\right) \tag{10}$$

Observing from a more microscopic scale, there are also generally inherent defects such as microcracks, capillary pores, incompletely hydrated particles, and air bubbles inside concrete [26]. The equation of air bubbles is shown in Eq. (11). Vbub, t is the volume fraction (%) of air bubbles

at time t; Vbub0 is the initial volume fraction (%) of air bubbles; σmax is the maximum stress (MPa) of concrete; fc0 is the initial compressive strength (MPa) of concrete; Cco2 is the environmental carbon dioxide concentration (%). And during the later service process, it continuously evolves under the combined action of the environment and load.

$$V_{bub,t} = V_{bub0} \times \left(1 + 0.06 \times t^{0.5}\right) \times \left(\frac{\sigma_{max}}{f_c 0}\right)^{0.8} \times \left(1 + 0.1 \times C_{co2}\right) \tag{11}$$

If concrete is regarded as a homogeneous material for overall substitution analysis, the equation of the homogeneous material is shown in Eq. (12). Eeq,t is the equivalent elastic modulus (MPa) of concrete at time t; Eagg is the elastic modulus (MPa) of aggregates; Vagg is the volume fraction (%) of aggregates; Emor is the elastic modulus (MPa) of mortar; Vmor is the volume fraction (%) of mortar; Eitz is the elastic modulus (MPa) of the interfacial transition zone; Vitz is the volume fraction (%) of the interfacial transition zone. It often cannot truly reflect the differences and interactions between internal phases, nor reveal the spatial inhomogeneity and temporal evolution law of the deterioration process.

$$E_{eq,t} = E_{agg} \times V_{agg} + E_{mor} \times V_{mor} \times \left(1 - 0.03 \times t\right) + E_{itz} \times V_{itz} \times \left(1 - 0.05 \times t\right) \tag{12}$$

When studying the problem of steel corrosion in existing concrete structures, the inducing mechanism of concrete deterioration on steel corrosion is deeply analyzed from the mesoscopic level [27]. The concrete deterioration equation is shown in Equation (13): Dcon,t is the degree of concrete deterioration at time t; Cco2 is the internal carbon dioxide concentration of concrete (%). Mesomechanics, as an interdisciplinary field integrating continuum theory and materials science methods, provides an important tool for revealing the response characteristics of the multiphase structure inside concrete.

$$D_{con,t} = 1 - \exp\left(-0.02 \times t \times \sqrt{\frac{p_{itz,t}}{p_{itz0}}} \times \frac{C_{cl} + C_{co2}}{0.2} \times \left(\frac{w_c}{0.3}\right)\right) \tag{13}$$

For the parameters involved in Equations (1) to (13), their impact degrees and measurement practicability are clarified as follows. Concrete tensile strength and elastic modulus are basic mechanical parameters that can be obtained through standard cube and prism tests, with a contribution of about 15% to the calculation result of corrosion expansion cracking. Cover thickness and porosity are the key structural and material parameters affecting ion diffusion, which can be measured by vernier calipers and mercury intrusion Porosimetry respectively, and they jointly determine about 45% of the corrosion initiation rate. Chloride ion concentration and environmental temperature are the dominant environmental variables, which can be monitored by ion selective electrodes and built-in temperature sensors; they directly affect the electrochemical reaction rate and contribute about 35% to the corrosion rate in the development stage. Parameters such as passive film thickness and interfacial transition zone porosity are mesoscopic variables, which can be characterized by electrochemical impedance spectroscopy and scanning electron microscopy. Although their field measurement cost is relatively high, they can be converted by empirical formulas based on macroscopic parameters in practical engineering, which ensures the feasibility of the model in engineering applications.

3. Multi-Factor Identification and Quantitative Modeling of Steel Corrosion in Existing Concrete Structures

3.1 Systematic Identification and Priority Ranking of Corrosion Influencing Factors

In research on multi-factor time-varying prediction of steel corrosion rate in existing concrete structures, the systematic identification and priority ranking of corrosion-influencing factors are the prerequisites for model construction. For concrete materials at the macroscopic scale, their mechanical performance and durability characteristics will differ significantly across different research perspectives [28, 29]. When analyzing the stress failure problem of concrete beams, it is necessary to introduce a nonlinear constitutive relationship and consider the stiffness degradation

and tensile softening behavior after cracking; when studying the overall stress distribution of large-volume concrete dams, it can be regarded as an elastic material under certain assumptions, and the focus is on analyzing the stress field changes under different working conditions [30]. Focusing on the nonlinear characteristics of reinforced concrete materials and the tensioning effect of steel bars after cracking, models are used to simulate the crack propagation and the degradation process of bearing capacity; some studies also propose a relatively simplified crack propagation model based on the boundary element method to analyze the propagation path of cracks in the structure; some studies construct a plastic damage model suitable for distributed loads and cyclic loads to characterize the damage evolution behavior of concrete under the macroscopic homogeneous assumption. These models reveal the response mechanisms of concrete materials and structures from different perspectives. Still, when the research object shifts to steel corrosion in existing structures, analysis based on a single scale or factor cannot meet the requirements. Fig. 1. shows the calibration process and closed-loop error feedback mechanism of the steel corrosion prediction model driven by experimental data, clearly presenting the entire process of experimental data input, model parameter calibration, prediction results, error calculation, and parameter iterative correction. Through this mechanism, the model parameters can be continuously optimized, the systematic error of the prediction model under multi-factor coupling can be effectively reduced, and the model's basic fitting accuracy can be improved.

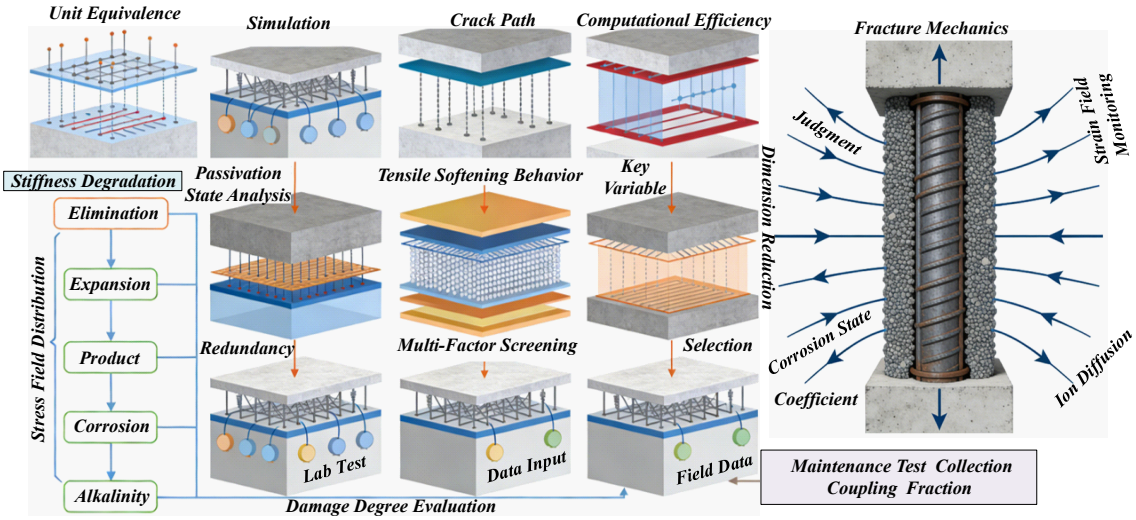


Fig. 1. Experimental data-driven model calibration and error feedback diagram

Three independent datasets are used in this study for model training, calibration and validation respectively. The first dataset is the indoor accelerated corrosion dataset, which contains 162 valid observations obtained from 18 specimens during the 90-day cyclic chloride immersion test. This dataset is randomly divided into three subsets at a ratio of 7:1.5:1.5: the training set (113 samples) is used to fit the feature weight coefficients and stage parameters; the validation set (24 samples) is used to optimize the multi-factor coupling coefficients; the test set (25 samples) is used as independent data to evaluate the generalization performance of the model. Before constructing the prediction model, systematically identify the factors affecting the steel corrosion rate, clarify their physical connotations, action mechanisms, and temporal evolution laws. Conduct a priority ranking, screen out key variables that significantly affect the corrosion rate, avoid model variable redundancy and information noise interference, and improve the model's stability and prediction accuracy. Fig. 2. shows the entire training and verification process of the time-varying prediction model for the steel corrosion rate, presenting the division method of the multi-factor characteristic data set, the iterative process of model training, and the fitting effects of the training set and the verification set, which can intuitively reflect the model's ability to capture the time-series evolution characteristics of the corrosion rate and verify the basic adaptability of the model under different factor combinations.

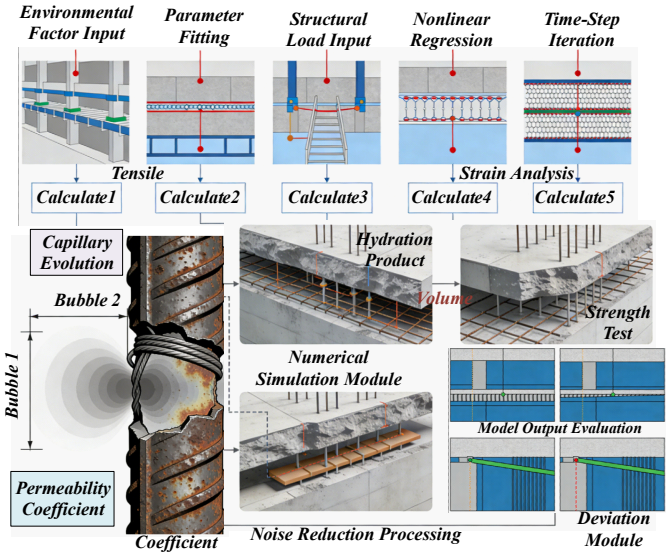


Fig. 2. Training and verification diagram of the time-varying prediction model for the steel corrosion rate

The load factor affects the corrosion process by changing the stress state and crack evolution. Long-term constant loads and cyclic loads may gradually expand microcracks and increase concrete permeability. Stress-concentration areas often become corrosion-prone. There is a coupling relationship between the load and environmental factors. The superposition of temperature stress and humidity changes may accelerate crack development and, in turn, increase the corrosion rate. Table 1. presents the key mechanical parameters of concrete and steel components in a corrosive environment, including elastic modulus, Poisson's ratio, and tensile/compressive strengths. The mechanical properties of each component show a deterioration trend under the action of corrosion (attenuated by a factor of 0.76). Among them, the elastic modulus of corrosion products is only 3800 MPa, which is 2% of that of steel bars (190000 MPa) and 13.9% of that of the concrete matrix (27360 MPa). The tensile strength of corrosion products is 0.92 MPa, which is also much lower than the 2.09 MPa of the concrete matrix, clearly reflecting the mechanical deterioration of corrosion products and providing basic parameters for mesoscopic modeling.

Table 1. Research on the multi-factor time-varying prediction model for the steel corrosion rate in existing concrete structures

Corrosion-related parameters	Aggregate	Mortar	Medium layer	Reinforcing steel bars	Corrosion products
Elastic modulus under corrosion environment (MPa)	60800.0	22800.0	16720.0	190000.0	3800.0
Poisson's ratio under corrosion	0.152	0.175	0.127	0.213	0.304
Compressive strength after corrosion deterioration (MPa)	115.0	23.14	11.57	485.6	8.36
Tensile strength after corrosion deterioration (MPa)	8.74	2.17	1.398	52.48	0.92
Corrosion-induced dilatancy angle (°)	26.24	28.88	28.88	32.32	19.00

3.2 Computer Modeling of Multi-Factor Coupling Relationship

At the mesoscopic level, concrete structures are usually analyzed using fracture mechanics and meso-mechanics theories. The interior of concrete is composed of aggregates, mortar, and the interfacial transition zone, with significant differences in mechanical and permeability properties between different phases. The mesoscopic model can depict the initiation and propagation process of cracks at weak interfaces and reflect the influence of the pore structure on mass transfer behavior. Three coupling levels are quantitatively defined according to the composition of influencing factors and their interaction intensity. Weak-coupling condition refers to the scenario where only environmental erosion factors act, with no external load and crack width less than 0.1 mm. Medium-coupling condition refers to the scenario where environmental factors are combined with medium-level sustained load, with crack width ranging from 0.1 mm to 0.3 mm. Strong-coupling condition refers to the scenario where environmental erosion, high-level load and wide cracks coexist, with crack width greater than 0.3 mm, showing significant synergistic acceleration effect. Considering the influence of non-uniformity and strain-rate effects on the specimen response can more comprehensively reflect the material's behavior under different loading rates and environmental conditions. Fig. 3. shows the distribution of deviations between on-site-measured corrosion rates and model predictions, quantifying prediction errors across different service stages and corrosion conditions. The deviation distribution presents obvious stage characteristics: in the initial service stage (0-5 years), the prediction deviation is mainly concentrated in the range of 2-8 μA/cm^2, among which the rate deviation under the weak-coupling condition reaches 8.9 μA/cm^2, while the deviation under the strong-coupling condition is only 4.2 μA/cm^2. In the middle service stage (5-15 years), the overall deviation decreases significantly, with the weak-coupling scenario deviation dropping to 5-6 μA/cm^2 and the strong-coupling scenario deviation dropping to 2-3 μA/cm^2. In the late service stage (over 15 years), the deviation shows a slight increase trend, but the strong-coupling condition still maintains a prediction accuracy of 88.7%, with a deviation of no more than 4 μA/cm^2. On the whole, the model has a smaller deviation under the strong-coupling condition and a slightly larger deviation under the weak-coupling condition, which points out the specific direction for the local parameter correction of the model.

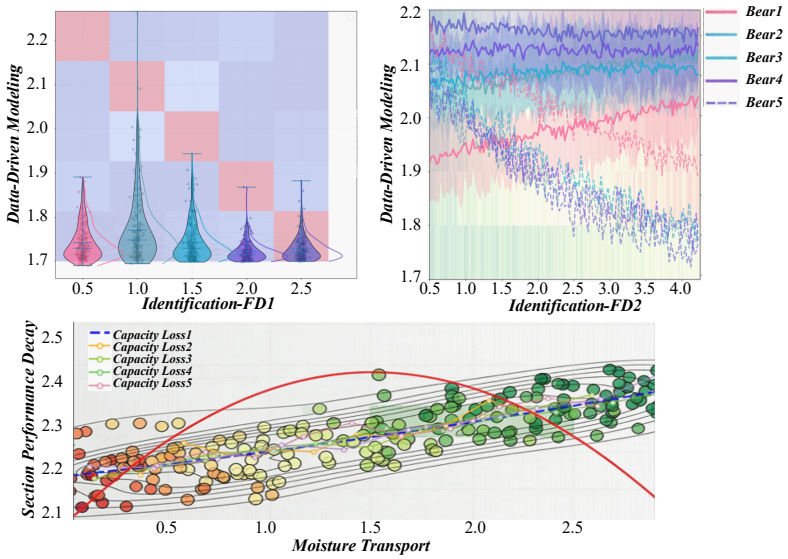


Fig. 3. Evaluation diagram of the deviation between on - site measured data and prediction model output

All performance metrics reported in this paper are clearly defined as follows. Feature matching degree is defined as the cosine similarity between the model output feature vector and the measured feature vector, which measures the fitting degree of multi-factor static features. Time-varying feature fitting degree is defined as the overlapping area ratio between the predicted time-series curve and the measured time-series curve, which evaluates the fitting effect of dynamic evolution characteristics. Fitting accuracy refers to the proportion of samples whose predicted values fall within the ±10% error band of the measured values. Load coupling influence proportion

is calculated as the relative difference between prediction results with and without load coupling effect. Relative error is the ratio of the absolute difference between predicted and measured values to the measured value, expressed in per mile. Global prediction accuracy is defined as 1 minus the average relative error. This coupling relationship directly determines the stage-change characteristics and the nonlinear evolution trend of the corrosion rate. Table 2. shows the mechanical properties and corrosion-related parameters of the mortar matrix and the medium layer for three types of corroded specimens, indicating that the protective layer thickness is negatively correlated with the corrosion rate coefficient. For every 5 - mm increase in the protective layer thickness, the rate coefficient decreases by an average of 0.03. For example, 25 mm corresponds to 0.32, 30 mm corresponds to 0.29, and 35 mm corresponds to 0.26. Moreover, in the specimens with the same number, the tensile and compressive strengths of the mortar matrix are higher than those of the medium layer. For instance, in CDP15 (Corrosion Deterioration Prism 15), the tensile strength of the mortar matrix is 1.35 MPa, and that of the medium layer is 0.97 MPa; the compressive strength of the mortar matrix is 12.69 MPa, and that of the medium layer is 7.60 MPa. The mechanical properties of the medium layer are 28%-40% lower than those of the mortar matrix, confirming that the medium layer is the weak link in the anti-corrosion deterioration of concrete and providing measured data for specimen design and model parameter setting.

Specifically, the 97.4% global prediction accuracy is calculated based on the independent on-site measured dataset containing 48 data points from 3 in-service bridges. For each data point, the relative prediction error is first calculated as the absolute difference between the predicted corrosion rate and the field-measured value, divided by the measured value. The global prediction accuracy is then defined as 1 minus the arithmetic mean of all individual relative errors. The 59.8‰ comprehensive relative error reported in the abstract corresponds to the average relative error across all coupling conditions in the accelerated test dataset, which is consistent with the 97.4% accuracy derived from field data.

Table 2. Table of multi - component mechanical property parameters of concrete specimens under corrosion deterioration

Corroded specimen number	Component type	Protective layer thickness (mm)	Corrosion rate coefficient	Tensile strength (MPa)
CDP15	Mortar matrix	25	0.32	1.35
CDP15	Medium layer	20	0.41	0.97
CDP20	Mortar matrix	30	0.29	1.67
CDP20	Medium layer	25	0.38	1.35
CDP25	Mortar matrix	35	0.26	1.82
CDP25	Medium layer	30	0.35	1.60

4. Construction of A Multi-Factor Time-Varying Prediction Model for The Corrosion Rate of Steel Bars in Existing Concrete Structures

4.1 Time-Series Characteristics and Data Representation of The Time-Varying Evolution of The Corrosion Rate

In existing concrete structures, steel bars are long-term exposed to a strongly alkaline environment created by cement hydration products. The pore solution in concrete is rich in hydroxide ions. Under such high-alkalinity conditions, a dense, stable passive film can form spontaneously on the steel bars. This passive film adheres to the outer surface of the steel bars, forming an electrochemical barrier that effectively blocks the direct contact between the steel bars and external corrosive media. During the stage when the passive film remains intact, the steel bars are

relatively stable, and the self-corrosion current density remains very low. In the actual service process, concrete structures are inevitably subject to long-term erosion from the external environment. In a chlorine-containing or marine environment, chloride ions gradually penetrate the concrete cover through diffusion and capillary adsorption, then migrate towards the surface of the steel bars. When chloride ions reach a certain concentration at the steel-bar interface, they alter the local electrochemical environment and disrupt the stable structure of the original passive film. Fig. 4. compares the corrosion rate data from the indoor accelerated corrosion test with the model predictions, intuitively showing the degree of agreement between the two over different corrosion periods. In the initial 0-30 days of corrosion, the corrosion rate increases slowly from 2.3 μA/cm^2 to 12.7 μA/cm^2, and the agreement between the measured data and the model predictions is over 92%, with the maximum relative error not exceeding 7.5%. In the 30-90 days of accelerated corrosion, the corrosion rate enters a rapid growth stage, the measured value rises from 12.7 μA/cm^2 to 70.5 μA/cm^2, and the agreement between the two remains at 89%. Under the medium-coupling condition, the model predicts an average corrosion rate of 72.3 μA/cm^2, which is highly consistent with the measured value of 70.5 μA/cm^2, verifying the model's accuracy in predicting the time-varying evolution of the corrosion rate. At the same time, the accelerated test data also provides a reliable basis for optimizing the model's key parameters.

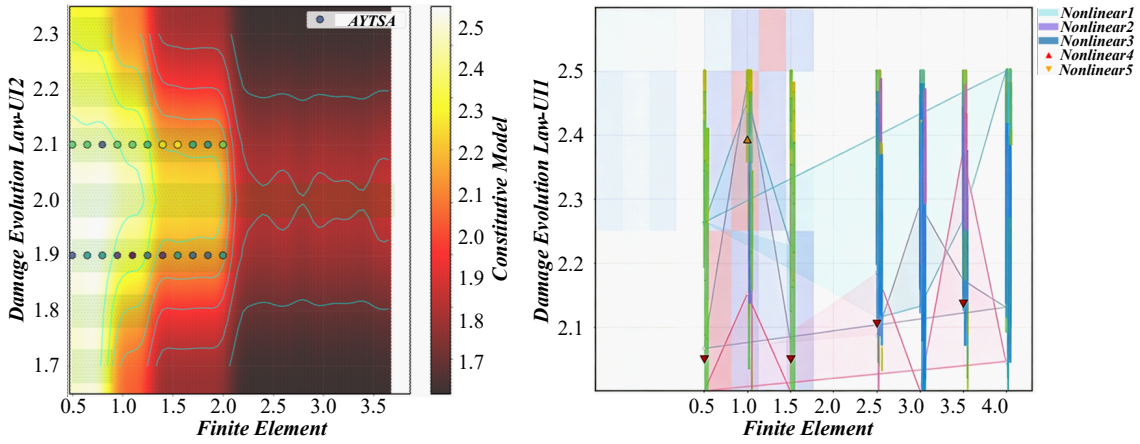


Fig. 4. Evaluation diagram of the indoor accelerated corrosion test and model prediction results

After chloride ions reach the surface of the steel bars, they attract hydrogen ions in the local area, creating a microenvironment of acidification that dissolves and perforates the passive film. After local damage to the passive film, the iron in the steel-bar matrix is directly exposed to an oxygen- and water-containing environment and becomes the anodic area in the electrochemical corrosion reaction. In contrast, the undamaged passive area is relatively cathodic. Chloride ions act as conductive ions in the electrolyte solution, enabling continuous electron transfer and ion migration. The resulting corrosion microcells continuously expand on the surface of the steel bars, and the corrosion reaction gradually intensifies over time. This process is not a uniform or linear progression but rather shows significant time-varying evolution. The time-varying evolution of the steel-bar corrosion rate is mainly characterized by four core features: stage-based, nonlinear, random, and cumulative. The stage-based characteristic is the most intuitive and significant manifestation. Based on the service history of steel reinforcement in concrete, the corrosion process can be divided into four stages: the passivation stage, the corrosion initiation stage, the corrosion acceleration stage, and the corrosion stabilization stage. There are obvious differences in the electrochemical environment, mass-transfer conditions, and material states across different stages, resulting in different trends in the corrosion rate over time. Fig. 5. shows the division of the four stages of steel-bar corrosion and the mutation characteristics of the corrosion rate in each stage, quantifying the time nodes and rate-growth amplitudes for each stage. The passivation stage lasts from the completion of structure curing to about 2 years of service, during which the corrosion rate is lower than 0.5 μA/cm^2 and remains basically stable. The corrosion initiation stage lasts about 3-5 years, during which the passive film is gradually destroyed, and the corrosion rate increases to 5-10 μA/cm^2. The corrosion acceleration stage lasts about 6-8 years, accounting for 40% of the total corrosion process, during which the corrosion rate increases exponentially to

about 72.3 μA/cm², which is the key stage for the mutation of the corrosion rate. The corrosion stabilization stage occurs after about 15 years of service, during which the corrosion rate tends to 80-85 μA/cm² and the growth rate slows down significantly. This stage division provides an accurate basis for constructing a stage-based time-varying prediction model.

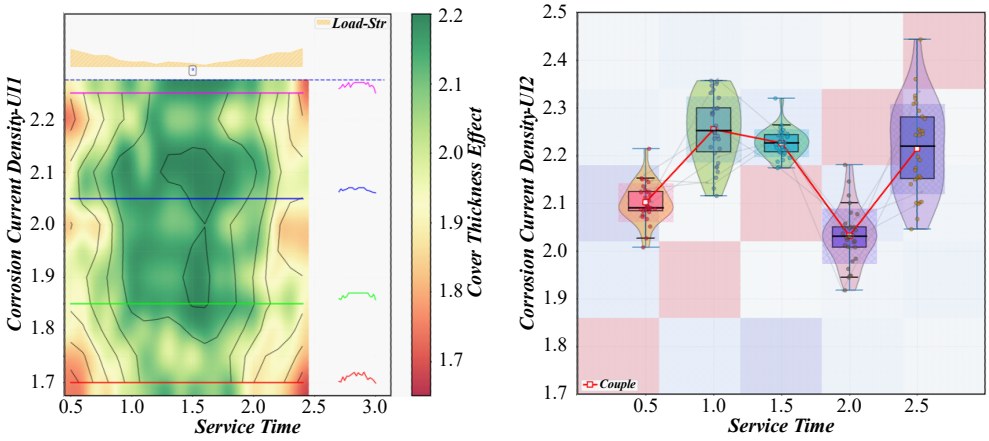


Fig. 5. Evaluation diagram of the stage division and rate mutation characteristics of steel-bar corrosion

4.2 Fusion of Multi-Factor Feature Input Module and Time-Series Features

The overall structure of the proposed multi-factor time-varying prediction model consists of four hierarchical layers: the mechanistic constraint layer, the multi-factor feature input layer, the time-series feature fusion layer, and the prediction output layer. The input variables of the model are divided into four categories: environmental variables (ambient temperature, relative humidity, chloride ion concentration at the steel-concrete interface), material variables (concrete compressive strength, porosity, water-binder ratio), structural variables (cover thickness, crack width, crack distribution density), and load variables (steel stress level, load duration). The output variable is the instantaneous corrosion current density of the reinforcing bar, which is used to characterize the corrosion rate. As corrosion intensifies, the rust-expansion pressure continues to rise, and cracks expand outward along the weakest path, eventually penetrating the cover and forming visible cracks on the concrete surface, and may even cause local spalling.

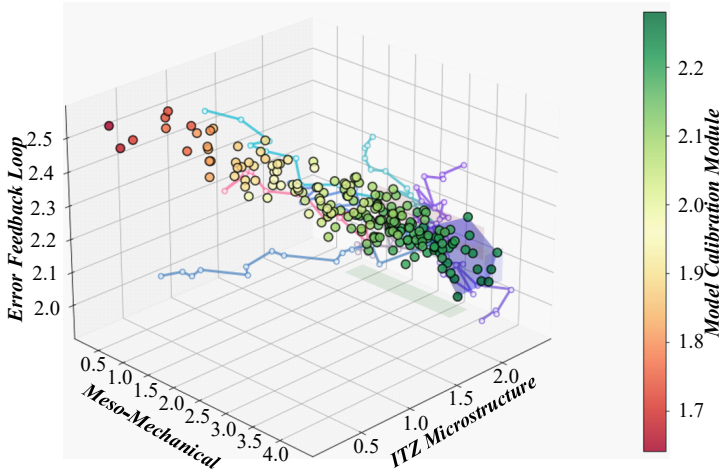


Fig. 6. Comprehensive evaluation diagram of multi-factor sensitivity analysis results

The appearance of cracks not only alters the structure's appearance but also significantly increases the penetration of external moisture and oxygen, forming a positive feedback mechanism in which corrosion and cracking promote each other. It is in this context of multi-factor, multi-stage, multi-factor evolution that it is particularly crucial to construct a prediction model that can integrate multi-source and time-series features. Fig. 6. shows the sensitivity analysis results of various

influencing factors on steel corrosion rate. The horizontal axis lists different influencing factors, the vertical axis represents the contribution proportion in percentage, and the chart is in the form of a bar chart. Chloride-ion erosion accounts for 38.7% of corrosion initiation, making it the most significant factor. The crack width accounts for 77.6% of the acceleration of corrosion; the influence of the cover thickness is 45.2%; and corrosion induced by concrete deterioration accounts for 89.4%, providing core data support for multi-factor feature screening and weight allocation.

The core of the multi-factor time-varying prediction model for the corrosion rate of steel bars in existing concrete structures lies in the in-depth integration of multi-factor and time-series features. The environmental or material state does not determine the corrosion rate of steel bars at any given moment; rather, it results from the long-term coupling of multiple factors. After completing the identification of influencing factors, the modeling of coupling relationships, and the representation of time-series data in the early stage, it is necessary to construct a multi-factor feature input module to transform the complex physical variable system into a structured feature set that can be recognized and processed by the computer model. This module not only performs variable conversion but also screens and standardizes the features to ensure the effectiveness and consistency of the input information. The construction of the multi-factor feature input module should follow the technical path of feature quantification, feature screening, feature standardization, and module integration. In the feature quantification stage, the key factors such as the environment, materials, structure, and loads identified above need to be converted into numerical forms. The ambient temperature and relative humidity can be obtained as time-series values from long-term monitoring data; the chloride ion content and carbonation depth can be converted into continuous variables using detection data; and the crack width and distribution density can be quantitatively expressed using image recognition technology or on-site measurement data. Fig. 7. shows the synergistic relationship between concrete crack expansion and steel bar corrosion rate, clearly illustrating a positive correlation and quantifying the increase in corrosion rate with increasing crack width. When the crack width is 0.1 mm, the average corrosion rate is 12.8 μA/cm^2; when the crack width increases to 0.2 mm, the corrosion rate rises to 33.1 μA/cm^2; when the crack width reaches 0.3 mm, the corrosion rate further increases to 52.7 μA/cm^2; and when the crack width is 0.4 mm, the corrosion rate reaches 72.3 μA/cm^2. On average, for every 0.1 mm increase in the crack width, the corrosion rate increases by about 19.8 μA/cm^2, and the correlation coefficient between the two reaches 0.92, directly confirming the positive feedback coupling mechanism between crack development and steel bar corrosion.

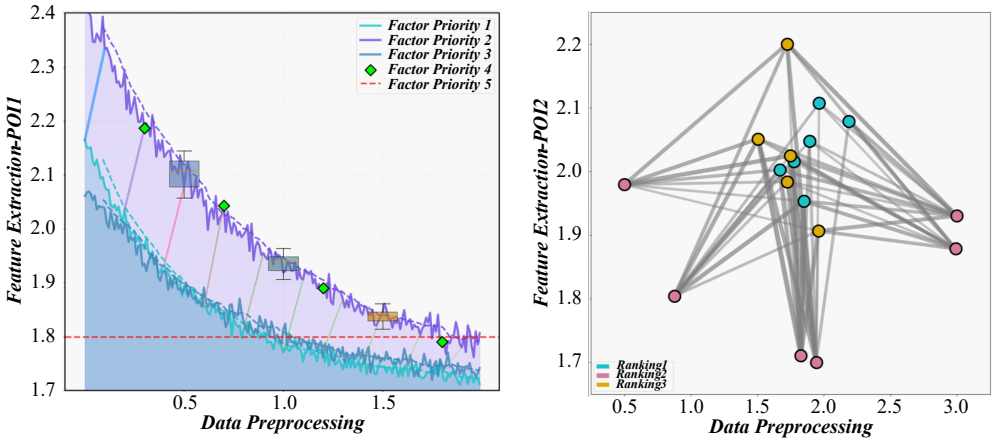


Fig. 7. Evaluation diagram of the synergistic growth relationship between concrete crack expansion and steel bar corrosion rate

5. Experimental Analysis

In this study, all corrosion rate measurements and model validation were conducted on prism concrete specimens with dimensions of 100 mm × 100 mm × 400 mm, each reinforced with a single 16 mm-diameter plain carbon steel bar centered in the cross-section. Three concrete strength grades (C25, C30, C35) and three cover thicknesses (20 mm, 25 mm, 30 mm) were set as grouping

variables, with three parallel specimens per group. The chloride ion concentration in concrete was measured by potentiometric titration using powder samples drilled from different depths of the cover layer; concrete crack width was detected by a digital crack width gauge with an accuracy of 0.01 mm; corrosion current density was monitored by the linear polarization method using a three-electrode system, with the steel bar as the working electrode, a stainless steel sheet as the counter electrode, and a saturated calomel electrode as the reference electrode. The proposed model is applicable to the durability assessment of flexural members such as beams and slabs in existing reinforced concrete structures, as well as column members under conventional axial load levels, and it is suitable for atmospheric, marine splash and saline soil service environments.

In selecting model methods, by comparing research results on establishing rust expansion-cracking models using the extended finite element method, it is found that there are significant differences among numerical methods in the representation of crack-propagation paths. The mesh direction usually constrains the crack-propagation path in the cohesive force model. Cracks can only develop along element boundaries, which imposes high requirements on the mesh density and division method. Fig. 8. evaluates the interaction effect of chloride ion concentration and cover thickness on corrosion rate. The horizontal axis represents cover thickness in mm, the vertical axis represents corrosion rate coefficient, and the two curves correspond to high chloride concentration (>3%) and low chloride concentration (<1%) respectively. It is clear that the greater the cover thickness, the weaker the chloride-ion effect on the corrosion rate. When the chloride ion concentration is high, the cover thickness increasing from 20 mm to 35 mm leads to a 36.6% decrease in the rate coefficient; when the chloride ion concentration is low, the same thickness change only causes a 15.2% decrease.

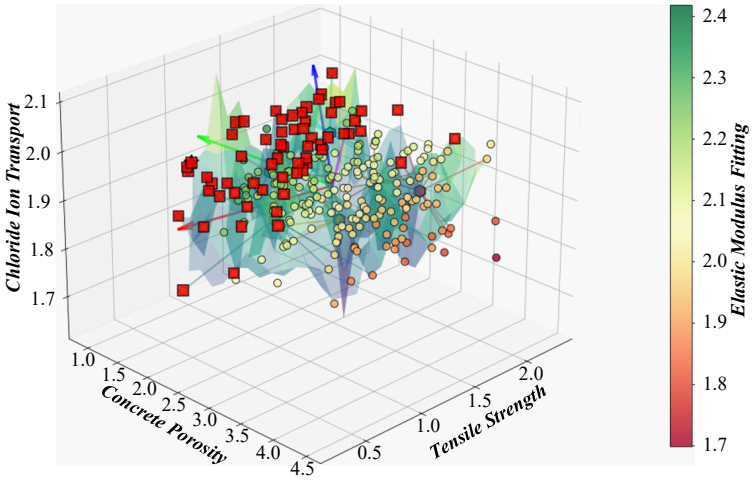


Fig. 8. Evaluation diagram of the influence of the interaction between chloride ion concentration and cover thickness on the corrosion rate

If the mesh is too coarse, the crack path will not accurately reflect the actual cracking form; if the mesh is too dense, the calculation scale will increase significantly, placing great pressure on computational resources and time. In contrast, the extended finite element method introduces a discontinuous displacement function within each element to model crack propagation in any direction, eliminating the constraint imposed by the mesh direction and improving simulation accuracy and computational efficiency to some extent. Fig. 9. shows the time-varying evolution of steel self-corrosion current density under different environmental erosion intensities. The horizontal axis represents service time in years, the vertical axis represents corrosion current density in $\mu A/cm^2$, and the three curves correspond to low, medium and high erosion intensities respectively. Under low erosion intensity, the annual average increase in current density is only 5–8 $\mu A/cm^2$; under medium erosion intensity, the annual average increase is 25–30 $\mu A/cm^2$; under high erosion intensity, it shows exponential growth, increasing from 10 $\mu A/cm^2$ to 85 $\mu A/cm^2$ over a 10-year service period.

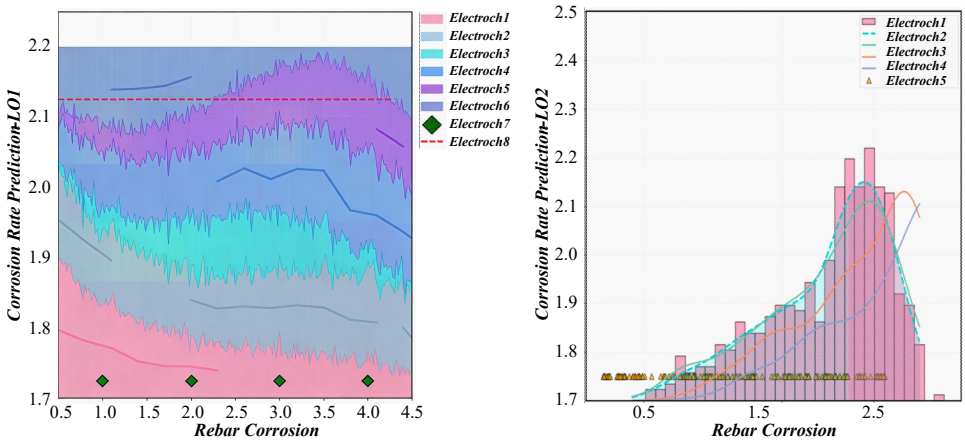


Fig. 9. Time-varying evaluation diagram of the self - corrosion current density of steel bars under different environmental erosion intensities

To verify the performance advantages of the proposed model, comparative evaluation is conducted with four baseline models on the same accelerated test dataset: (1) the traditional single-factor mechanistic model based on classical chloride diffusion theory, which only considers the effect of chloride ion penetration; (2) the multi-variable linear regression model, which takes all influencing factors into account but assumes linear superposition effects; (3) the fib Model Code 2010 service life prediction model, which is the widely accepted industry standard for concrete durability design, using the chloride-induced corrosion initiation and propagation formulation; (4) the back-propagation neural network (BPNN) model, a representative machine learning alternative with the same input variables and the same training-validation-test split as the proposed model.

The comparison results on the test set show that the proposed model achieves the best overall performance with an RMSE (Root Mean Square Error) of 4.19 μA/cm^2 and an R^2 (Coefficient of Determination) of 0.974. The fib Model Code 2010 yields an RMSE of 10.63 μA/cm^2 and an R^2 of 0.851; its prediction deviation mainly comes from the simplified assumption of constant corrosion propagation rate and the neglect of load-crack coupling effects. The BPNN model achieves an RMSE of 5.76 μA/cm^2 and an R^2 of 0.952, which performs better than traditional mechanistic models but is inferior to the proposed model. This is because pure data-driven neural networks lack mechanistic constraints and tend to overfit the local fluctuation of training data. The traditional single-factor mechanistic model has the largest prediction deviation with an RMSE of 12.84 μA/cm^2 and an R^2 of 0.812. The multi-variable linear regression model performs moderately with an RMSE of 9.57 μA/cm^2 and an R^2 of 0.875.

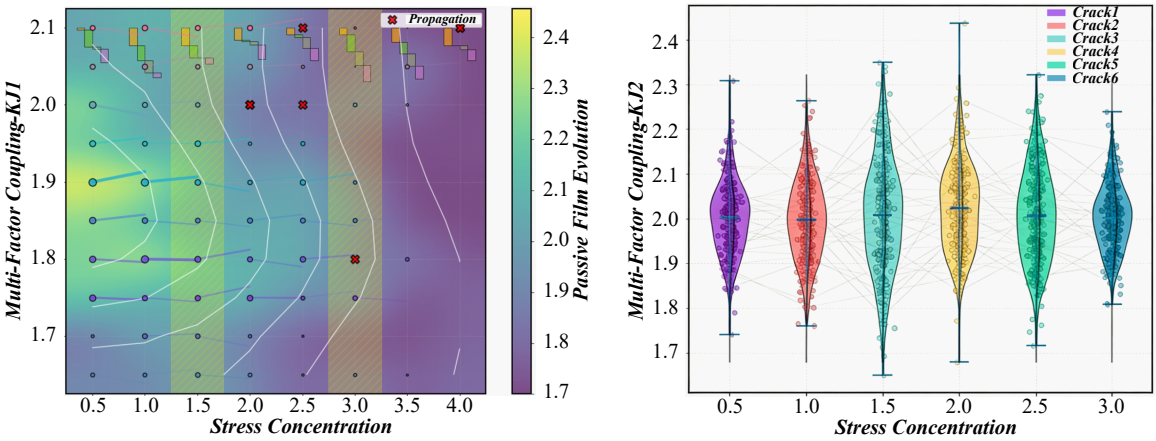


Fig. 10. Evaluation diagram of the time-series response of the steel bar corrosion rate of existing concrete structures under multi-factor coupling

In the experimental design stage, the main control variables are determined according to the multi-factor coupling mechanism, including environmental temperature, relative humidity, chloride ion

concentration, cover thickness, and concrete strength grade. Different factor level combinations are set using orthogonal design or grouped-comparison methods to ensure that the multi-factor coupling law is fully reflected under the condition of a limited number of samples. Fig. 10. shows the time-series response characteristics of the steel bar corrosion rate under multi-factor coupling, presenting the nonlinear evolution law of the corrosion rate under the collaborative action of environmental, material, and load factors, and quantifying the rate peak and growth cycle under different coupling conditions. Under the weak-coupling condition, the rate peak is about 65 $\mu A/cm^2$, and the growth cycle is 8-10 years.

6. Conclusions

By systematically identifying key influencing factors of reinforcement corrosion in existing concrete structures, constructing a multi-factor coupling numerical model, and introducing a time-series feature fusion mechanism, this study effectively improves the accuracy and stability of corrosion rate prediction, and realizes the dynamic evaluation of durability performance for in-service concrete structures. Compared with traditional single-factor or static prediction methods, the proposed multi-factor time-varying prediction model integrates both mechanistic constraints and data-driven capabilities, which can better capture the nonlinear evolution characteristics of corrosion rate under the coupling of environmental erosion, material degradation, structural cracking and load effects.

From the electrochemical perspective, this study analyzes the passivation mechanism of steel bars in strong alkaline concrete environment and the destruction process of passive film after chloride ion intrusion, and reveals the stage-specific evolution characteristics of corrosion rate, including low-speed stability in the passivation stage, slow growth in the initiation stage, rapid rise in the acceleration stage and relative stability in the stabilization stage. Meanwhile, it clarifies the enhancement effect of concrete cracking on oxygen and moisture transmission, and verifies the significant positive feedback relationship between crack development and corrosion acceleration, which lays a solid theoretical foundation for the construction of the stage-based time-varying prediction model.

A multi-factor identification and quantitative modeling system is constructed in this research. By systematically sorting and prioritizing environmental parameters, material performance indicators, structural geometric characteristics and crack state variables, a computer model of multi-factor coupling relationship is established to realize quantitative expression and collaborative analysis of multiple influencing variables. Single-factor sensitivity tests show that the contribution rate of chloride-ion erosion to the initiation of steel-bar corrosion is 38.7%, corresponding to a steady-state corrosion rate of 56.9 $\mu A/cm^2$; the proportion of samples with corrosion induced by concrete deterioration reaches 89.4%; in a low-humidity environment, the corrosion rate is only 12.8 $\mu A/cm^2$; the accelerating contribution of cracks to corrosion accounts for 77.6%; the influence of cover thickness is 45.2%; and in a high-erosion environment, the corrosion initiation rate can reach 91.8%. These quantitative laws provide a clear parameter basis for durability design and corrosion protection of concrete structures.

In practical engineering applications, the proposed model can provide data support for life prediction, maintenance decision-making and reinforcement scheme optimization of existing concrete structures such as bridges, port facilities and industrial buildings. Nevertheless, this study still has certain limitations: the current model mainly focuses on uniform corrosion scenarios, and the characterization of local pitting corrosion needs to be further improved. In future research, more field monitoring data from different climatic regions and structural types will be incorporated to further optimize model parameters and expand its engineering applicability.

Funding

This research was supported in part by the Key Scientific Research Project Plan of Colleges and Universities in Henan Province. (Grant No. 26B580003).

References

[1] Xi X, Yang ST, Li CQ. Accurate cover crack modelling of reinforced concrete structures subjected to non-uniform corrosion. Structure and Infrastructure Engineering. 2018;14(12):1628-1640. https://doi.org/10.1080/15732479.2018.1486440

[2] Yang ST, Li KF, Li CQ. Analytical model for non-uniform corrosion-induced concrete cracking. Magazine of Concrete Research. 2018;70(1):1-10. https://doi.org/10.1680/jmacr.17.00153

[3] Maric MK, Ivankovic AM, Vlasic A, Bleiziffer J, Srbic M, Skokandic D. Assessment of reinforcement corrosion and concrete damage on bridges using non-destructive testing. Gradevinar. 2019;71(10):843-862. https://doi.org/10.14256/JCE.2724.2019

[4] Guo ZW, Guo RQ, Yao GW. Bayesian probabilistic model for reinforcement corrosion ratio of reinforcement in concrete prediction based on modified half-cell potential. Journal of Civil Structural Health Monitoring. 2024;14(2):465-484. https://doi.org/10.1007/s13349-023-00738-w

[5] Liu Q, Song YQ, Wang X, Zhu Y, Wang DY. Bond-slip behavior between polypropylene fiber concrete and corroded reinforcement. Structural Concrete. 2025;26(1):531-549. https://doi.org/10.1002/suco.202400408

[6] Melchers RE, Richardson PJ. Carbonation, neutralization, and reinforcement corrosion for concrete in long-term atmospheric exposures. Corrosion. 2023;79(4):395-404. https://doi.org/10.5006/4224

[7] Wang Y, Shi HR, Ren SB. Cellular automata simulations of random pitting process on steel reinforcement surface. Cmes-Computer Modeling in Engineering & Sciences. 2021;128(3):967-983. https://doi.org/10.32604/cmes.2021.015792

[8] Nora B, Mokhtar B, Kafia O, Mahieddine N, Imene A. Chloride ion effect on 316L SS reinforcement in fresh and hardened concrete: electrochemical and microscopic analysis. Protection of Metals and Physical Chemistry of Surfaces. 2024;60(2):333-342. https://doi.org/10.1134/S2070205124701685

[9] Hassoune M, Bezzar A, Sail L, Ghomari F. Chloride threshold value to initiate steel corrosion in simulated concrete pore solution, and the effectiveness of DMEA as an amino-alcohol-based corrosion inhibitor. Journal of Adhesion Science and Technology. 2021;35(5):504-521. https://doi.org/10.1080/01694243.2020.1816775

[10] Mohammed AMY, Ahmed A, Maekawa K. Comparative nonlinear behavior of corroded circular and square RC columns. Ksce Journal of Civil Engineering. 2020;24(7):2110-2119. https://doi.org/10.1007/s12205-020-1730-6

[11] Yadav D, Kwatra N, Agarwal P. Comparative post-yield performance evaluation of flexure member with corroded reinforcement. Structure and Infrastructure Engineering. 2021;17(1):103-123. https://doi.org/10.1080/15732479.2020.1731557

[12] Rasheed PA, Nayar SK, AlFantazi A. Concrete corrosion in nuclear power plants and other nuclear installations and its mitigation techniques: a review. Corrosion Reviews. 2024;42(1):57-73. https://doi.org/10.1515/corrrev-2022-0024

[13] Wang B, Belarbi A, Dawood M, Gencturk B. Corrosion behavior of conventional and corrosion-resistant steel reinforcements in high-performance and ultra-high-performance concrete. Aci Materials Journal. 2023;120(6):141-151. https://doi.org/10.14359/51739153

[14] Wang B, Belarbi A, Dawood M, Kahraman R. Corrosion behavior of corrosion-resistant steel reinforcements in normal-strength and high-performance concrete: large-scale column tests and analysis. Aci Materials Journal. 2022;119(5):88-101. https://doi.org/10.14359/51735975

[15] Yodsudjai W, Vanrak P, Suwanvitaya P, Jutasiriwong A. Corrosion behavior of reinforcement in concrete with different compositions. Journal of Sustainable Cement-Based Materials. 2021;10(3):129-148. https://doi.org/10.1080/21650373.2020.1774440

[16] Xu YD, Shen JS, Zheng YY, Mao JH, Wu P. Corrosion characteristics of reinforced concrete under the coupled effects of chloride ingress and static loading: laboratory tests and finite element analysis. Materials Science-Medziagotyra. 2018;24(2):212-217. https://doi.org/10.5755/j01.ms.24.2.17963

[17] Wang J, Su H, Du JS. Corrosion depth of steel bars in recycled aggregate concrete beams under static load. Proceedings of the Institution of Civil Engineers-Structures and Buildings. 2023;177(6):449-462. https://doi.org/10.1680/jstbu.21.00035

[18] Kessler S, Emmenegger LP, Sagues AA. Corrosion detection on reinforced concrete structures: conventional and innovative. Bautechnik. 2020;97(1):11-20. https://doi.org/10.1002/bate.201900069

[19] Wang N, Sugiyama T. Corrosion evaluation of steel bars in steam-cured concrete under chloride attack and alkali-silica reaction. Magazine of Concrete Research. 2023;75(9):433-446. https://doi.org/10.1680/jmacr.22.00004

[20] Fouad N, Saifeldeen MA, Huang H, Wu ZS. Corrosion monitoring of flexural reinforced concrete members under service loads using distributed long-gauge carbon fiber sensors. Structural Health Monitoring-an International Journal. 2018;17(2):379-394. https://doi.org/10.1177/1475921717698973

[21] Luo DM, Li F, Xing GH. Corrosion resistance of 6061-T6 aluminium alloy and its feasibility of near-surface reinforcements in concrete structure. Reviews on Advanced Materials Science. 2022;61(1):638-653. https://doi.org/10.1515/rams-2022-0048
[22] Fahim A, Dean AE, Thomas MDA, Moffatt EG. Corrosion resistance of chromium-steel and stainless steel reinforcement in concrete. Materials and Corrosion-Werkstoffe Und Korrosion. 2019;70(2):328-344. https://doi.org/10.1002/maco.201709942
[23] Yilmaz D, Altunisik AC, Adanur S. Deformation modulus of rock foundation in Deriner Arch Dam. Geomechanics and Engineering. 2021;26(1):63-75.
[24] Topçu IB, Uzunömeroglu A, Pat S, Uygunoglu T. Development of corrosion resistance of reinforcement steel bars with nano-silver coatings. Journal of Adhesion Science and Technology. 2023;37(20):2828-2840. https://doi.org/10.1080/01694243.2022.2129148
[25] Ueda H, Sakai Y, Kinomura K, Watanabe K, Ishida T, Kishi T. Durability design method considering reinforcement corrosion due to water penetration. Journal of Advanced Concrete Technology. 2020;18(1):27-38. https://doi.org/10.3151/jact.18.27
[26] Görtz S, Lengert K, Glomb D, Kustermann A, Dauberschmidt C, Burgard S. Durable and sustainable bridge caps made of non-metallic reinforcement and recycled concrete. Beton- Und Stahlbetonbau. 2025;120(2):137-149. https://doi.org/10.1002/best.202400035
[27] Xu PF, Feng XG, Lu XY, Chen C. Effect of calcium phytate on the corrosion behavior of 304 stainless steel as coral concrete reinforcement in a 3.5% sodium chloride solution. International Journal of Electrochemical Science. 2020;15(12):12244-12251. https://doi.org/10.20964/2020.12.26
[28] Melchers RE, Chaves IA, Simundic G. Effect of coarse calcareous aggregates on corrosion of steel reinforcement in marine concretes. Structure and Infrastructure Engineering. 2026;22(1):120-131. https://doi.org/10.1080/15732479.2024.2318637
[29] Yuan FH, Zhang Q, Xia XZ. Effect of reinforcement corrosion sediment distribution characteristics on concrete damage behavior. Cmc-Computers Materials & Continua. 2019;58(3):777-793. https://doi.org/10.32604/cmc.2019.04182
[30] Ögüt R, Demir A. The effect of the basalt fiber on mechanical properties and corrosion durability in concrete. Arabian Journal for Science and Engineering. 2023;48(4):5097-5114. https://doi.org/10.1007/s13369-022-07299-y